The crystal and magnetic structures of $LaCa_2Fe_3O_8$ and $NdCa_2Fe_3O_8$

2009 J. Phys.: Condens. Matter 21 124206

(http://iopscience.iop.org/0953-8984/21/12/124206)

J. Phys.: Condens. Matter **21** (2009) 124206 (8pp) doi:10.1088/0953-8984/21/12/124206

The crystal and magnetic structures of $LaCa_2Fe_3O_8$ and $NdCa_2Fe_3O_8$

J M Hudspeth[1], D J Goossens[1,2,4], A J Studer[3], R L Withers[2] and L Norén[2]

[1] Department of Physics, The Australian National University, Canberra, ACT 0200, Australia
[2] Research School of Chemistry, The Australian National University, Canberra, ACT 0200, Australia
[3] Bragg Institute, Australian Science and Technology Organisation, Lucas Heights, NSW 2234, Australia

E-mail: goossens@rsc.anu.edu.au

Received 3 November 2008, in final form 19 December 2008
Published 25 February 2009
Online at stacks.iop.org/JPhysCM/21/124206

Abstract

The crystal and magnetic structures of $LaCa_2Fe_3O_8$ and $NdCa_2Fe_3O_8$ have been established using a combination of x-ray, neutron and electron diffraction.

It was already considered likely that $LaCa_2Fe_3O_8$ and $NdCa_2Fe_3O_8$ were made up of stacked perovskite-like layers of FeO_6 octahedra, with every third layer being replaced by a layer of tetrahedrally coordinated Fe, rather like a variation on the Brownmillerite ($Ca_2Fe_2O_5$) structure type. We have gone further and determined a likely space group for this Grenier phase and determined the magnetic structure of the compounds at room temperature.

The space group is found to be $P2_1ma$ (b axis as the long axis), and the crystal structure has been refined, subject to the stacking faulting along the long axis that is apparent in electron diffraction patterns.

The magnetic structure of $LaCa_2Fe_3O_8$ is shown to consist of antiferromagnetically ordered Fe^{3+} ions on a collinear G-type antiferromagnetic structure, with the magnetic moments most likely (anti)parallel with the c axis, and of magnitude $3.4 \pm 0.2\mu_B$ ($3.6 \pm 0.2\mu_B$ for $NdCa_2Fe_3O_8$). The result is reasonable given the magnetic structures of the end members of the $La_{1-x}Ca_xFeO_3$ series, $LaFeO_3$ ($x = 0$) and $Ca_2Fe_2O_5$ ($x = 1$).

(Some figures in this article are in colour only in the electronic version)

1. Introduction

Many materials of technological and scientific interest have structures which derive from, or are related to, the perovskite structure type. Once such family of materials is the rare earth calcium ferrates, $Ln_{1-x}Ca_xFeO_{3-\delta}$ (Ln = lanthanide ion). These materials are of interest for applications as catalysts for CO oxidation [1–4] and methane oxidation [5, 6, 3].

The magnetic properties of $LaCa_2Fe_3O_8$ have been investigated by Mössbauer spectroscopy and magnetometry measurements from 300 up to 1000 K [7]. Mössbauer measurements indicate that the compound is magnetically ordered at room temperature while magnetometry measurements were used to determine that this ordering is antiferromagnetic. The magnetic structure of the two end members, $LaFeO_3$ and $Ca_2Fe_2O_5$, are G-type antiferromagnetic and so $LaCa_2Fe_3O_8$ was also assumed to have this structure, although this has also not been confirmed until now. The Néel temperature of $LaCa_2Fe_3O_8$ was found to be 735 ± 10 K.

Considering the $Ln_{1-x}Ca_xFeO_{3-\delta}$ phase diagram for Ln = La as a function of x, it has been established that, depending on the details of sample preparation, Ca can be doped into the La sites while maintaining the perovskite-based structure up to a concentration of approximately $x = 0.5$ [8, 9]. Beyond this the material forms multi-phase samples except for the point phases, such as the Grenier phase, in which the layers of FeO_6 perovskite octahedra are interspersed with layers of FeO_4 tetrahedra, as exemplified by the other end member, $Ca_2Fe_2O_5$, of Brownmillerite structure type.

Hence, the intermediate phases between the end of the solid solution range and $Ca_2Fe_2O_5$ can generally be considered

[4] Author to whom any correspondence should be addressed.

as various stackings of octa- and tetrahedral layers. One such phase is the Grenier phase ($x = 2/3$ or, more precisely, $Ln$$Ca_2Fe_3O_8$) noted to form for the larger lanthanides, particularly La [10]. The phase is suggested to be a 2:1 stacking of octahedral, perovskite-like layers and tetrahedral layers.

Hence, while there are a range of results available on the Grenier phase, key quantitative results have been lacking; the space group has not been established (and therefore many details of the crystal structure are unknown) and the magnetic structure has not been determined. The work presented here remedies this. The phase is assigned a space group, and the first thorough structural refinements are discussed. The magnetic structure is established. These are useful results, not only because they provide the first detailed description of this phase, but also because the phase appears as an impurity phase in a range of syntheses attempting to stabilize the doped perovskite structure in rare earth calcium ferrates at high Ca doping levels. By characterizing it, the Grenier phase can be better fitted when analysing multi-phase samples.

2. Sample preparation

Polycrystalline samples of $LaCa_2Fe_3O_8$ and $NdCa_2Fe_3O_8$ were prepared from powders of $CaCO_3$ (99+%), $Fe(NO_3)_2{\cdot}9H_2O$ (99%) and rare earth oxides (99.9%).

The powders were dissolved in deionized water and a mixture of the metal oxides was formed via the decomposition of a citric acid–ethylene glycol sol–gel. The residues were pelleted and sintered at 1200 °C in air for up to three days with intermediate re-grinding and re-pelleting until no further reaction was evident by powder XRD.

3. Experimental details

3.1. XRD

Powder XRD measurements used a Siemens D5000 x-ray diffractometer at room temperature using Cu Kα radiation and a flat-plate sample holder. Data for structural refinement were collected over $2° \leqslant 2\theta \leqslant 120°$ with a step size of 0.02° and integration time of 9 s.

Further, a room temperature diffraction pattern of the La sample was collected using a Guinier–Hägg camera and Cu Kα_1 radiation. While not refinable, this data is of very high resolution and allows diffraction lines to be better resolved, allowing better insight into the reflection conditions of the materials. As the materials appear isostructural, and the La sample shows the greater orthorhombic splitting, it was the La sample that was chosen for this experiment.

3.2. Neutron powder diffraction

Neutron powder diffraction patterns were collected at room temperature for the two samples. The instrument used was the Wombat high intensity powder diffractometer at the Bragg Institute at the Australian Nuclear Science and Technology Organization (ANSTO) [11]. Because of the large d spacings possible for $0k0$-type reflections, a long wavelength—2.95 Å—was used and the radial collimator was removed from the instrument, as it obscures the lowest angle elements of the detector. Removal of the collimator has little effect on the resolution (because it is a radial collimator) but increases background. Increased background was dealt with by performing scans with an empty sample can, replicating all aspects of the experiment except scattering due to the sample. This allowed background subtraction to be performed.

3.3. Electron diffraction

Electron diffraction (ED) was carried out on $LaCa_2Fe_3O_8$ using a Philips EM 430 Transmission Electron Microscope operating at 300 kV. Samples suitable for TEM work were prepared by the dispersion of finely ground material onto a holey carbon film.

4. Results and discussion

4.1. Crystal structure

Figure 1 shows a selection of the electron diffraction patterns (EDPs) from $LaCa_2Fe_3O_8$ with figure 1(a) showing a [100] zone axis EDP. This zone axis EDP shows the b^* and c^* reciprocal axes and the $0kl$ reflections are all present and this rules out any out any conditions on these reflections of the form $k + l = 2n$. An arrow notes the streaking along b^*, indicating that there is stacking faulting between consecutive ac planes. The form of this faulting cannot as yet be specified exactly, but we note that the satellite 010 reflection is as sharp as the parent reflections in XRD and neutron diffraction, so the faulting is not on such a short length scale that the average unit cell consists of superimposed tetra- and octahedra.

It is worth noting that a tetrahedron may be considered as an octahedron with two O atoms removed. If the pair of atoms removed from the octahedron to form the tetrahedron is inconsistent from one tetrahedral layer to the next, stacking faulting would result, but without the need for erratic spacing of the tetrahedral layers (refer to figure 3(a)). The sharpness of the 010 reflection and some aspects of the refinement results discussed below suggest that this may be the case.

Having said that, there appear to be no purely Ca or Ln sites, but all A-sites are mixed to some degree; this is manifested in the diffraction patterns in the heights of the 'superlattice' peaks (those due to the tetrahedra and octahedra stacking, the 010 for example), and may indicate that either there *is* some cross-substitution, or that there is indeed some stacking faulting such that the spacing of the tetrahedral layers is erratic.

Figure 1(b) shows a [010] zone axis EDP. All the $h0l$ reflections with $k + l = 2n + 1$ are present which means these reflections must also be allowed. Although the reflections $h00$, h odd, and $00l$, l odd, seem to be absent in the XRD data, they are both present in this EDP as a result of multiple scattering. This can be explained by the reflections appearing in the EDPs because of double diffraction. The presence of the $h0l$, $h + l = 2n + 1$ reflections means that at least one of the $h00$, h odd, or $00l$, l odd, reflections must be allowed or the structure will not satisfy any of the orthorhombic space groups.

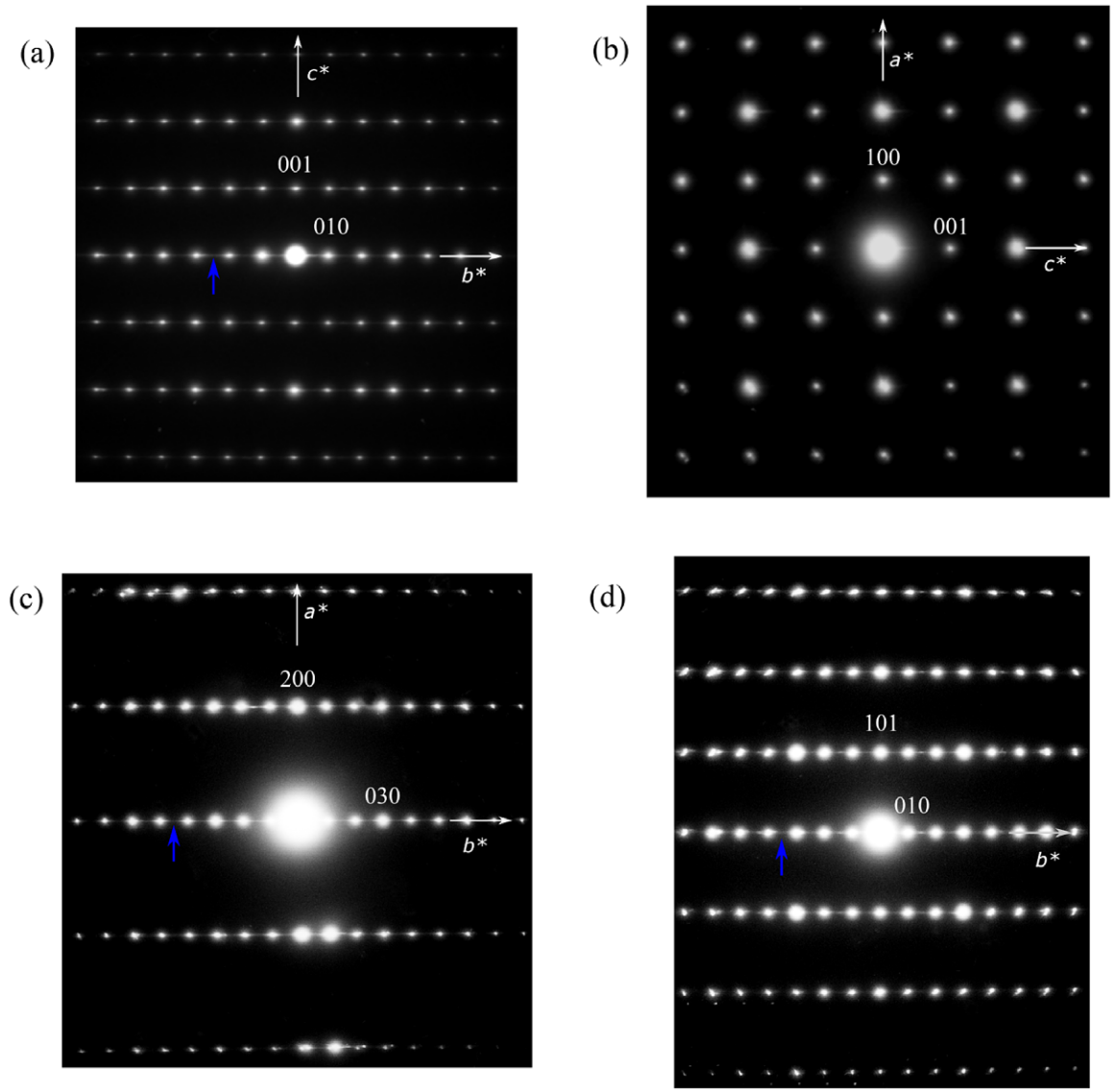

Figure 1. Electron diffraction patterns for $LaCa_2Fe_3O_8$ corresponding to the (a) [100], (b) [010], (c) [001] and (d) [101] zone axis orientations. In (c), the 010 reflection is present but is hidden by the central spot so the 030 reflection has been indicated instead. The only systematic absences are in (c) where the $hk0$, reflections are only present for $h = 2n$. The sharp streaking that can be seen along the b^* direction in (a) (indicated with an arrow) indicates significant stacking faulting along the b (long) axis, which will affect the refinement of the average structure. This streaking along b^* is also present in (c) and (d), but is more difficult to see because the Bragg spots are more intense.

Figure 1(c) shows that reflections of the form $hk0$, $h = 2n + 1$, are absent, in agreement with the Guinier–Hägg XRD result (below). This also means that $h00$, $h = 2n + 1$, reflections are really absent and are only visible in figure 1(b) because of double diffraction. The absence of these reflections means the $l00$, $l = 2n + 1$, are allowed and so there is no condition on these reflections. Figure 1(d) confirms that the cell is primitive since none of the hkl reflections are absent.

Combining these results, the only allowed space group symmetries are $P2_1ma$ (26), $Pm2a$ (28) or $Pmma$ (51).

Based on the model structure proposed for $LaCa_2Fe_3O_8$ it is possible to determine the approximate positions of the atoms in the unit cell. Both $Pm2a$ and $Pmma$ deny the atoms degrees of freedom they would be expected to exhibit based on the structures of related phases. This was borne out by structural refinement, which suggested that $P2_1ma$ was of the correct space group symmetry.

Figure 2 shows the powder diffraction pattern of $LaCa_2Fe_3O_8$ as measured using a Guinier–Hägg camera. The inset, the centre section of which has had its contrast enhanced, shows the 031 and 130 Bragg reflections, showing the lack of intensity in the 130 reflection, in accordance with the condition $h = 2n$ for the $hk0$ reflections deduced from the EDPs in figure 1.

Due to the nonlinearity of the response of photographic film with x-ray intensity, the Guinier data is not readily refinable using Rietveld refinement. However, data collected on a conventional θ–2θ powder x-ray diffractometer can be refined, though it is of lower resolution. Figures 4(a) and 5(a) show the patterns collected for $LaCa_2Fe_3O_8$ and $NdCa_2Fe_3O_8$.

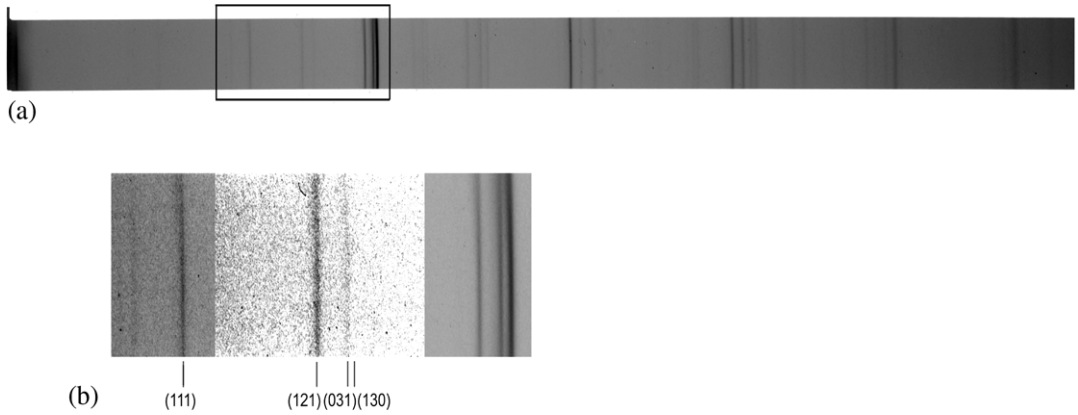

Figure 2. A powder diffraction exposure from $LaCa_2Fe_3O_8$ taken using a Guinier–Hägg camera. Note that the response of the film is not linear with x-ray intensity. The inset shows the 031/130 diffraction lines, demonstrating the high resolution of the Guinier–Hägg camera. It also suggests that the 130 line is absent, in accordance with one of the reflection conditions deduced from the EDPs, namely $h = 2n$ for the $hk0$ reflections.

Table 1. Unit cell parameters obtained from the Guinier–Hägg camera for $LaCa_2Fe_3O_8$ and from the simultaneous Rietveld refinement of the XRD and neutron diffraction data in $P2_1ma$ for $LaCa_2Fe_3O_8$ and $NdCa_2Fe_3O_8$.

Structure	Method	a (Å)	b (Å)	c (Å)	c/a	V (Å^3)
$LaCa_2Fe_3O_8$	Guinier	5.4674(7)	11.313(1)	5.5657(5)	1.0179(2)	344.25(6)
$LaCa_2Fe_3O_8$	Rietveld	5.468(6)	11.311(8)	5.568(7)	1.018(2)	344.4(6)
$NdCa_2Fe_3O_8$	Rietveld	5.453(9)	11.35(1)	5.529(9)	1.014(2)	342.2(8)

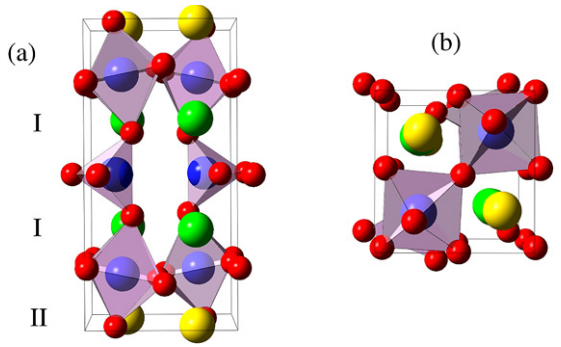

Figure 3. The unit cell of $LaCa_2Fe_3O_8$ with (a) the a axis into the page and (b) the b axis into the page, showing the positions of the ions from the structural refinement. The O^{-2} are on the corners of the octahedra and tetrahedra, while the Fe^{3+} are inside them. A-site layers are denoted I and II, with the I layers being Ca^{2+}-rich and the II layers being La^{3+}-rich, but the ordering is not perfect.

The fits, shown as solid lines through the points, are from Rietveld fits performed using FullProf [12, 13]. These fits result from a joint refinement in which the neutron diffraction and x-ray diffraction data were fitted jointly by a combined crystal structure and magnetic structure model.

Table 1 shows the key structural parameters for $LaCa_2Fe_3O_8$ and $NdCa_2Fe_3O_8$. Table 2 shows the refined atomic coordinates for $LaCa_2Fe_3O_8$ and table 3 shows the coordinates for $NdCa_2Fe_3O_8$.

Figures 4(b) and 5(b) show the diffraction patterns for $LaCa_2Fe_3O_8$ measured using 2.95 Å neutrons at room temperature. The solid line through the points gives the

Table 2. Atomic positions for the atoms in the asymmetric unit cell of $LaCa_2Fe_3O_8$ from the Rietveld structural refinement in $P2_1ma$. Occupancies are relative to that of the general position.

Site	Charge	x	y	z	Occ. (%)
O1	2−	0.03(3)	0.200(1)	0.015(4)	100
O2	2−	0.05(3)	0.147(2)	0.522(4)	100
O3	2−	−0.12(3)	0.500	0.097(5)	50
O4	2−	0.24(3)	0.000	0.193(5)	50
O5	2−	0.26(3)	0.363(1)	0.308(3)	100
Fe1	3+	0.268(3)	0.172(2)	0.240(2)	100
Fe2	3+	0.23(3)	0.500	0.200(3)	50
La1	3+	0.80(3)	0.000	0.259(3)	34.5(4)
Ca1	2+	0.80(3)	0.000	0.259(3)	15.5(4)
La2	3+	0.77(3)	0.317(1)	0.268(3)	15.5(4)
Ca2	2+	0.77(3)	0.317(1)	0.268(3)	84.5(4)

Table 3. Atomic positions for the atoms in the asymmetric unit cell of $NdCa_2Fe_3O_8$ from the Rietveld structural refinement in $P2_1ma$. Occupancies are relative to that of the general position.

Site	Charge	x	y	z	Occ. (%)
O1	2−	0.06(1)	0.200(1)	0.006(6)	100
O2	2−	0.05(1)	0.152(1)	0.486(5)	100
O3	2−	−0.088(7)	0.500	0.091(4)	50
O4	2−	0.35(1)	0.000	0.220(5)	50
O5	2−	0.327(8)	0.365(1)	0.333(2)	100
Fe1	3+	0.301(5)	0.165(2)	0.239(2)	100
Fe2	3+	0.253(7)	0.500	0.200(3)	50
Nd1	3+	0.826(7)	0.000	0.251(3)	23(2)
Ca1	2+	0.826(7)	0.000	0.251(3)	27(2)
Nd2	3+	0.792(6)	0.3143(8)	0.271(3)	27(1)
Ca2	2+	0.792(6)	0.3143(8)	0.271(3)	73(1)

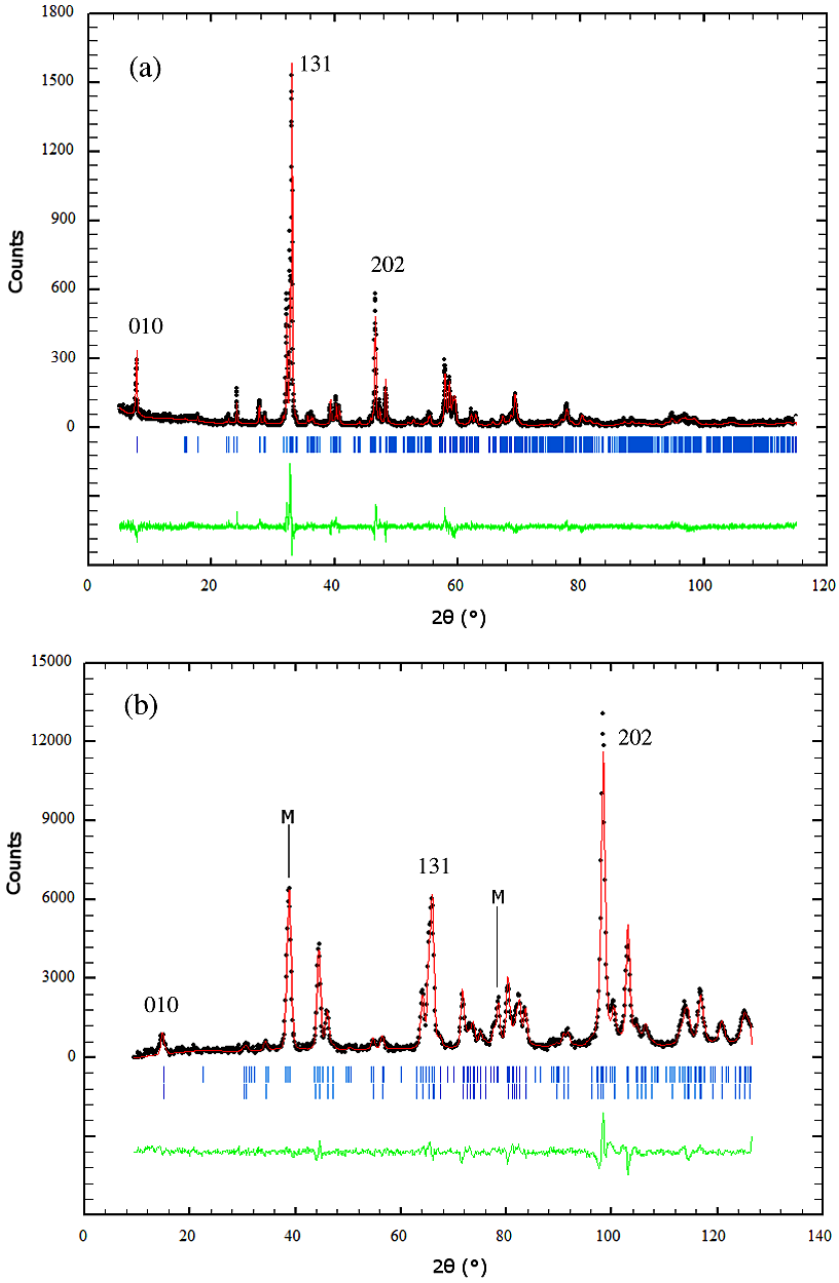

Figure 4. Simultaneous Rietveld refinement for $LaCa_2Fe_3O_8$ in $P2_1ma$ from (a) XRD data and (b) neutron data. The black circles are the data points, the lines through the points are the fits to the data, the lines below are the difference between the observed and calculated intensities and the vertical markers indicate the positions of the Bragg peaks. In (b) the top row of markers gives the magnetic Bragg peaks and the second row gives the structural Bragg peaks. The peaks marked with 'M' only have magnetic intensity. Miller indices for representative peaks, indexed on the crystal structural cell, have been noted to aid comparison. Goodness of fit, $S = R_{wp}/R_{exp} = 1.31$ (x-ray), 4.33 (neutron).

fit, the solid line below the difference between model and data. 'M' indicates diffraction features which are magnetic in origin and which do not strongly overlap with features due to the crystal structure. These reflections can be obtained with a magnetic cell which is doubled along b compared to the structural cell, and in which the magnetic moments are arranged antiferromagnetically and collinearly, such that all six nearest magnetic neighbours have opposite sign—that is, a G-type antiferromagnet. The cell doubling and a G-type magnetic structure result in reflections with non-integer Miller indices $k = k_{mag}/2$ which are purely magnetic for k_{mag} odd. Within the structural unit cell, the first magnetic peak 'M' in each plot is made up of the $0\frac{3}{2}1$ and $1\frac{3}{2}0$ reflections while the higher angle 'M' feature predominantly consists of the $1\frac{3}{2}2$ and $2\frac{3}{2}1$ magnetic reflections.

The ratio of the intensities of the two higher angle reflections ($1\frac{3}{2}2$ and $2\frac{3}{2}1$) in figures 4(b) and 5(b) is sensitive to the direction of the magnetic moments. Figure 6 plots this region of the data along with the same region simulated from three models in which the magnetic moments are aligned along the three crystallographic axes. The key magnetic reflections

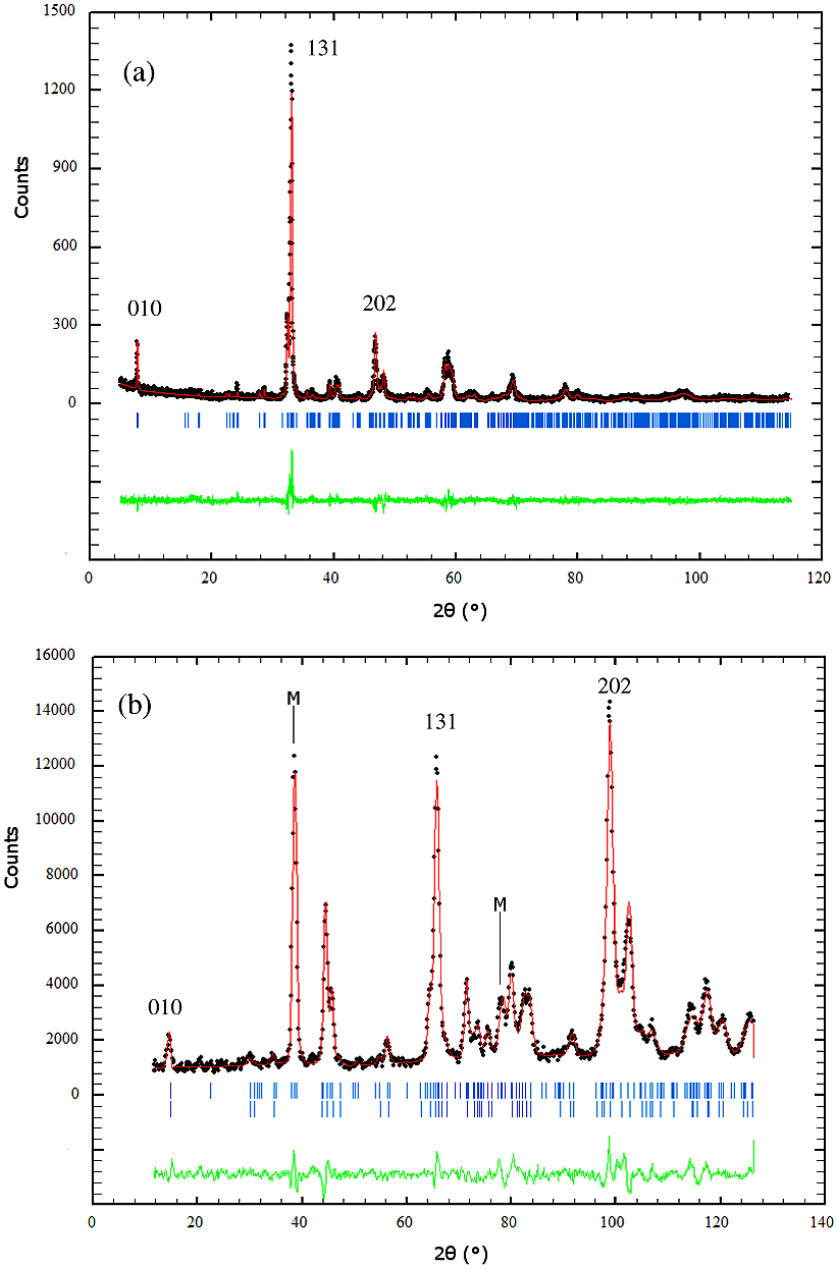

Figure 5. Simultaneous Rietveld refinement for $NdCa_2Fe_3O_8$ in $P2_1ma$ from (a) XRD data and (b) neutron data. The black circles are the data points, the lines through the points are the fits to the data, the lines below are the difference between the observed and calculated intensities and the vertical markers indicate the positions of the Bragg peaks. In (b) the top row of markers gives the magnetic Bragg peaks and the second row gives the structural Bragg peaks. The peaks marked with 'M' only have magnetic intensity. Miller indices for representative peaks, indexed on the crystal structural cell, have been noted to aid comparison. Goodness of fit, $S = R_{wp}/R_{exp} = 1.17$ (x-ray), 3.72 (neutron).

are the $1\frac{3}{2}2$ and the $2\frac{3}{2}1$. Plainly, aligning the moments (anti)parallel with the c axis gives the best model, and this was chosen as the starting configuration for magnetic Rietveld refinement.

These refinements suggested that the moment direction in $LaCa_2Fe_3O_8$ and $NdCa_2Fe_3O_8$ is indeed (anti)parallel with the c axis (the longer of the two short axes). The magnitude of the ordered moment is $3.4\pm0.2\mu_B$ in $LaCa_2Fe_3O_8$ and $3.6\pm0.2\mu_B$ in $NdCa_2Fe_3O_8$. This is of a similar scale to the ordered moments found in $LaFeO_3$ ($4.6\mu_B$ [14]) and Brownmillerite ($4.5\mu_B$ [15]), especially given that those results were from data measured at ~4 K ($T/T_C \sim 0$), whereas the results presented here are from data measured at ~295 K ($T/T_C \sim 0.4$), and the Brillouin curve for $S = 5/2$ shows a moment reduction of approximately 10% at $T/T_C \sim 0.4$ relative to $T = 0$. The moment direction in Brownmillerite is along a (the shortest axis in that material) and in $LaFeO_3$ it was not determined. Both are G-type antiferromagnets, so our results for the Grenier phase accord well with the behaviour across the series.

Interestingly, the model does not require the moments on the tetrahedrally coordinated Fe to be treated as different to

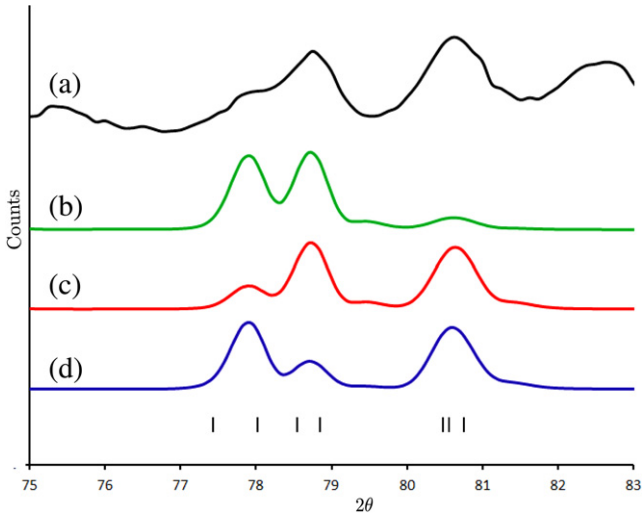

Figure 6. This plot shows scattering features from the $0\frac{5}{2}2$, $1\frac{3}{2}2$, $2\frac{5}{2}0$, $2\frac{3}{2}1$, $0\frac{9}{2}1$, 141 and $1\frac{9}{2}0$ magnetic reflections, indicated in that order by the black vertical markers (indexed on the structural cell—the magnetic cell being doubled along b relative to the crystal structural cell) from the neutron diffraction pattern of $LaCa_2Fe_3O_8$. Top line (a) shows the observed scattering. Line (b) shows a simulated magnetic scattering pattern if the magnetic moments form a collinear G-type structure (anti)parallel with the b axis, line (c) is the same result if the moments are along c and line (d) is for moments collinear with a. All intensity in the cluster of peaks $0\frac{5}{2}2$, $1\frac{3}{2}2$, $2\frac{5}{2}0$ and $2\frac{3}{2}1$ (around 78°) is magnetic in the observed data. This is a very small amount of nuclear scattering in the 141 reflection.

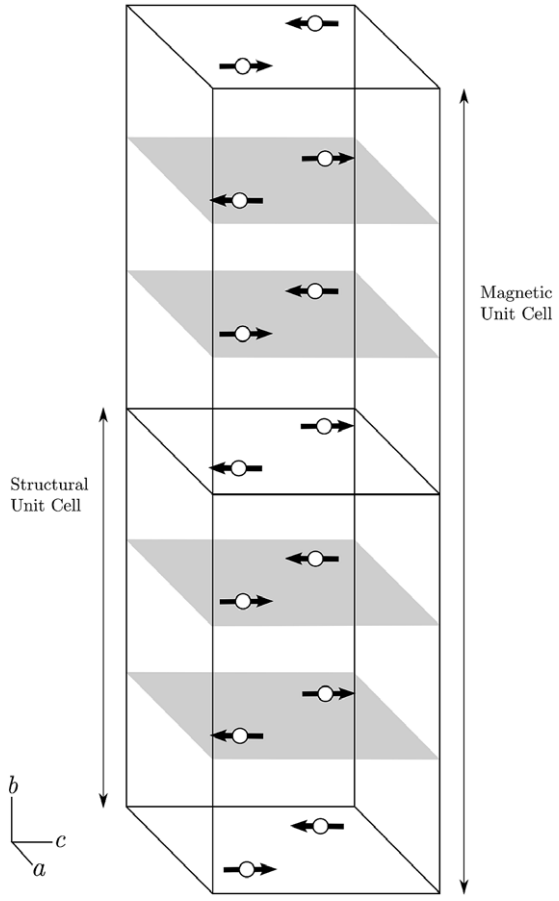

Figure 7. Schematic diagram of the magnetic structure of $LaCa_2Fe_3O_8$ and $NdCa_2Fe_3O_8$. Note the magnetic cell is doubled along b relative to the structural.

those in the octahedra. This reflects a number of issues; it could be related to the stacking faulting causing each Fe position to, in truth, be a superposition of octahedrally and tetrahedrally coordinated Fe, although this cannot be perfectly averaged out or the average structure would reflect this; and it may also reflect the limitations of the data.

Figure 7 shows a schematic digram of the magnetic structure of $LaCa_2Fe_3O_8$ and $NdCa_2Fe_3O_8$.

5. Conclusions

We have determined the crystal structure of the Grenier phase $LnCa_2Fe_3O_8$, Ln = La, Nd. We find it to be orthorhombic and to have a space group symmetry of $P2_1ma$ and unit cell parameters of $a = 5.4674(7)$ Å, $b = 11.313(1)$ Å and $c = 5.5657(5)$ Å for Ln = La and $a = 5.453(9)$ Å, $b = 11.35(1)$ Å and $c = 5.529(9)$ Å for Ln = Nd.

The Ca^{2+} ions are most concentrated in the layers adjacent to the tetrahedral Fe/O layers, while the Ln^{3+} ions tend to be found in the layers between the octahedral layers; however, the ordering is not perfect. Prominent streaking along b^* in the EDPs suggests stacking faulting along the b axis and it is likely that this faulting results in the mixing of Ca and Ln on the A-sites.

We find both materials to be G-type antiferromagnets, with the moments most likely directed along the c axis, and of magnitude $3.4 \pm 0.2\mu_B$ in $LaCa_2Fe_3O_8$ and $3.6 \pm 0.2\mu_B$ in $NdCa_2Fe_3O_8$ at room temperature. There is no discernible difference in the behaviour of the Fe^{3+} moments in the octahedral compared to the tetrahedral layers.

Acknowledgments

DJG gratefully acknowledges the support of the Australian Institute of Nuclear Science and Engineering (AINSE) through an AINSE Fellowship. We thank Ross Whitfield for help with neutron diffraction, Associate Professor Glen Stewart for Mössbauer measurements, which were not included in this paper, and Dr Michael James for helping initiate the research. RLW acknowledges the Australian Research Council for support in the form of an ARC discovery grant.

References

[1] Isupova L A, Yakovleva I S, Tsybulya S V, Boldyreva N N, Kryukova G N, Vlasov A A, Alikina G M, Ivanov V P and Sadykov V A 2000 *Kinet. Catal.* **41** 315–20

[2] Isupova L A, Tsybulya S V, Kryukova G N, Alikina G M, Boldyreva N N, Vlasov A A, Snegurneko O I, Ivanov V P, Kolomiichuk V N and Sadykov V A 2002 *Kinet. Catal.* **43** 140–9

[3] Isupova L A, Yakovleva I S, Rogov V A, Alikina G M and Sadykov V A 2004 *Kinet. Catal.* **45** 446–53

[4] Taguchi H, Masunaga Y, Hirota K and Yamaguchi O 2005 *Mater. Res. Bull.* **40** 773–80
[5] Ciambelli P, Cimino S, Lisi L, Faticanti M, Minelli G, Porta P and Pettiti I 2001 *Appl. Catal.* B **33** 193–203
[6] Sadykov V A, Isupova L A, Yakovleva I S, Alikina G M, Lukashevich A I and Neophytides S 2004 *React. Kinet. Catal. Lett.* **81** 393–8
[7] Grenier J C, Menil F, Pouchard M and Hagenmuller P 1977 *Mater. Res. Bull.* **12** 79–86
[8] Li J 1991 *Hyperfine Interact.* **69** 573–6
[9] Li J, Cai X and Wang T 1993 *Phys. Status Solidi* **176** 177–81
[10] Grenier J C, Darriet J, Pouchard M and Hagenmuller P 1976 *Mater. Res. Bull.* **11** 1219–26
[11] Studer A J, Hagen M E and Noakes T J 2006 *Physica* B **385/386** 1013–5
[12] Rodriguez-Carvajal J 2001 *Comm. Powder Diffr. Newsl.* **26** 12–9
[13] Rodriguez-Carvajal J 1993 *Physica* B **192** 55–69
[14] Koehler W C and Wollan E O 1957 *J. Phys. Chem. Solids* **2** 100–6
[15] Berastegui P, Eriksson S G and Hull S 1999 *Mater. Res. Bull.* **34** 303–14